Supplemental Materials

Prediction of superconductivity in metallic boron-carbon compounds from 0 to 100 GPa by high-throughput screening

Feng Zheng[1,2], Yang Sun[2*], Renhai Wang[3], Yimei Fang[2], Feng Zhang[4,5], Shunqing Wu[2*], Qiubao Lin[1*], Cai-Zhuang Wang[4,5], Vladimir Antropov[4,5], Kai-Ming Ho[4]

[1]School of Science, Jimei University, Xiamen 361021, China
[2]Department of Physics, OSED, Key Laboratory of Low Dimensional Condensed Matter Physics (Department of Education of Fujian Province), Jiujiang Research Institute, Xiamen University, Xiamen 361005, China.
[3]School of Physics and Optoelectronic Engineering, Guangdong University of Technology, Guangzhou 510006, China
[4]Department of Physics, Iowa State University, Ames, Iowa 50011, United States
[5]Ames Laboratory, U.S. Department of Energy, Ames, Iowa 50011, USA

SUPPLEMENTARY MATERIALS

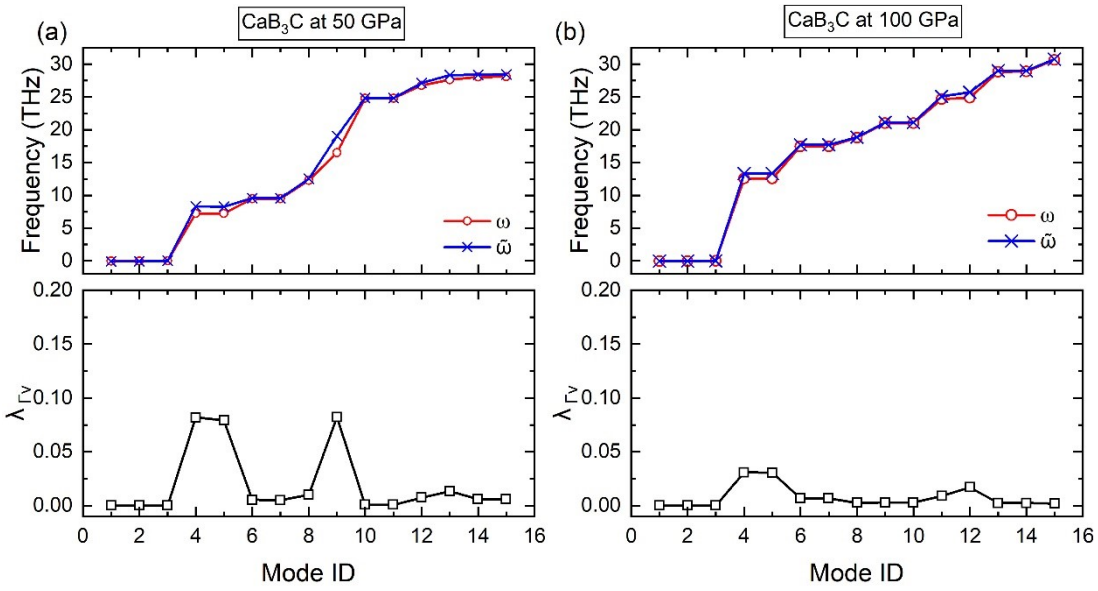

Fig. S1. The screened and unscreened phonon frequency (top panel) and zone-center EPC strength (bottom panel) in CaB_3C at (a) 50 and (b) 100 GPa.

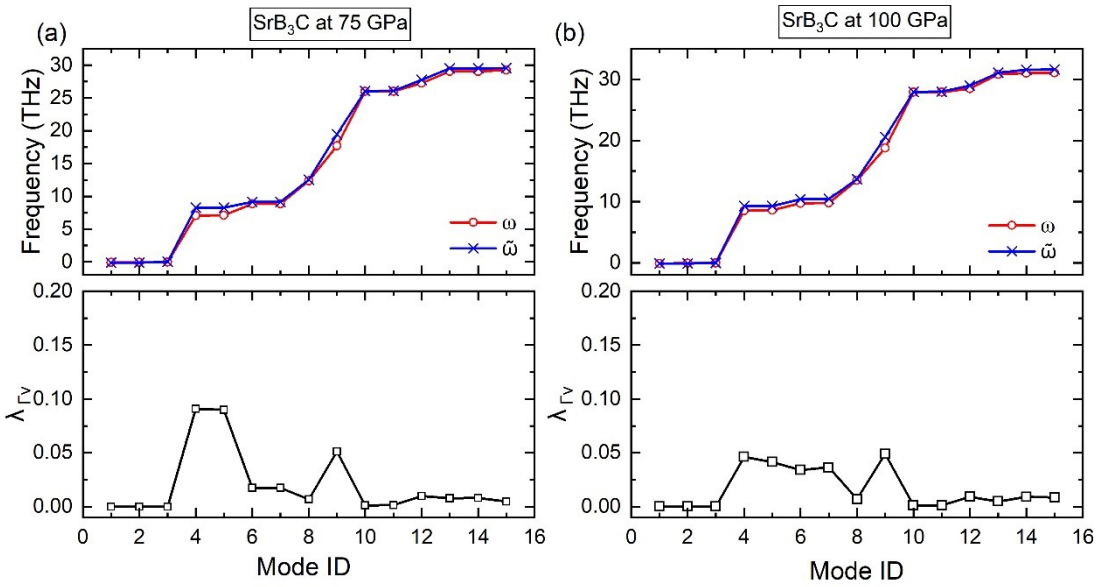

Fig. S2. The screened and unscreened phonon frequency (top panel) and zone-center EPC strength (bottom panel) in SrB_3C at (a) 50 and (b) 100 GPa.

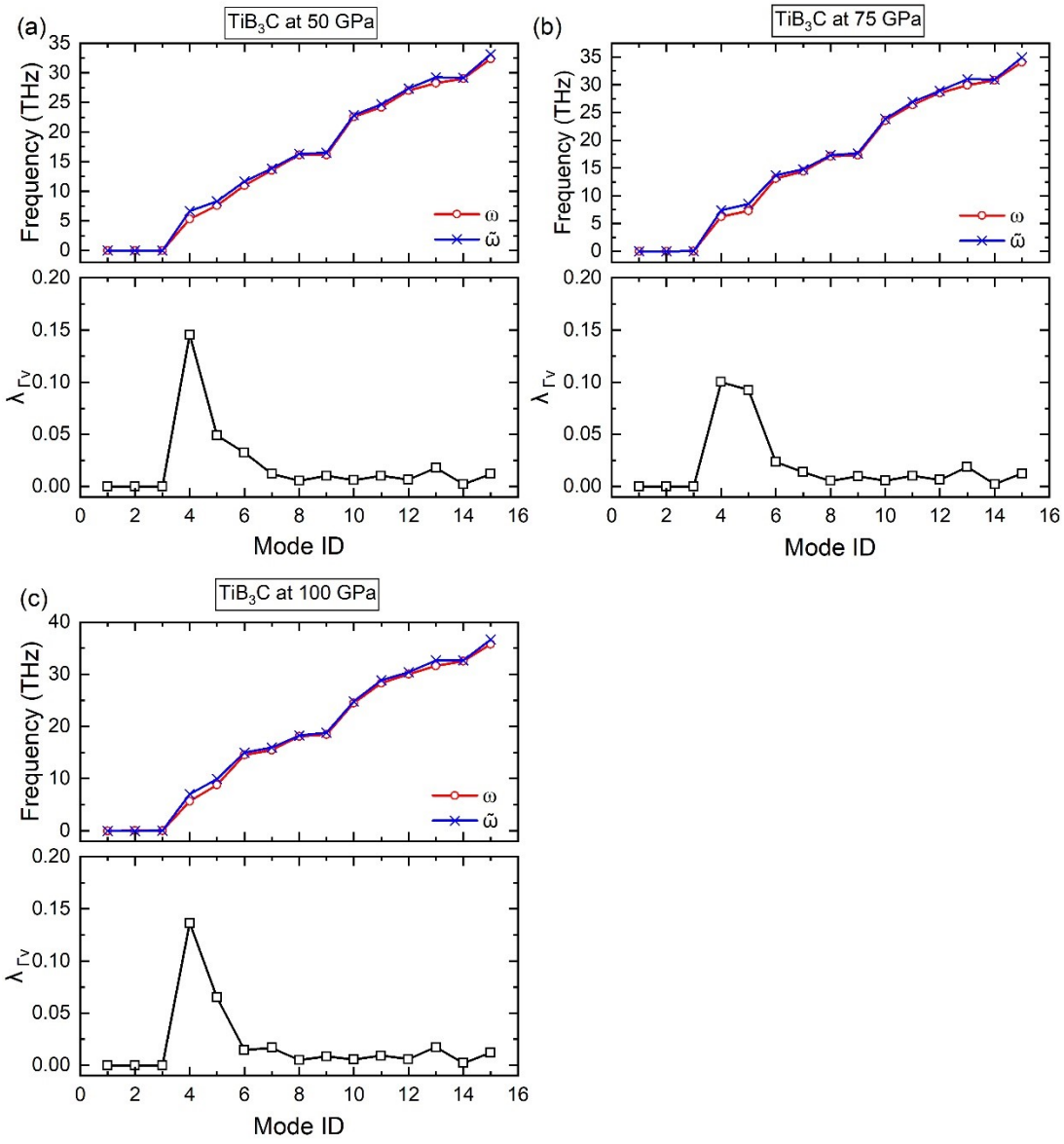

Fig. S3. The screened and unscreened phonon frequency (top panel) and zone-center EPC strength (bottom panel) in TiB_3C at (a) 50, (b)75 and (c) 100 GPa.

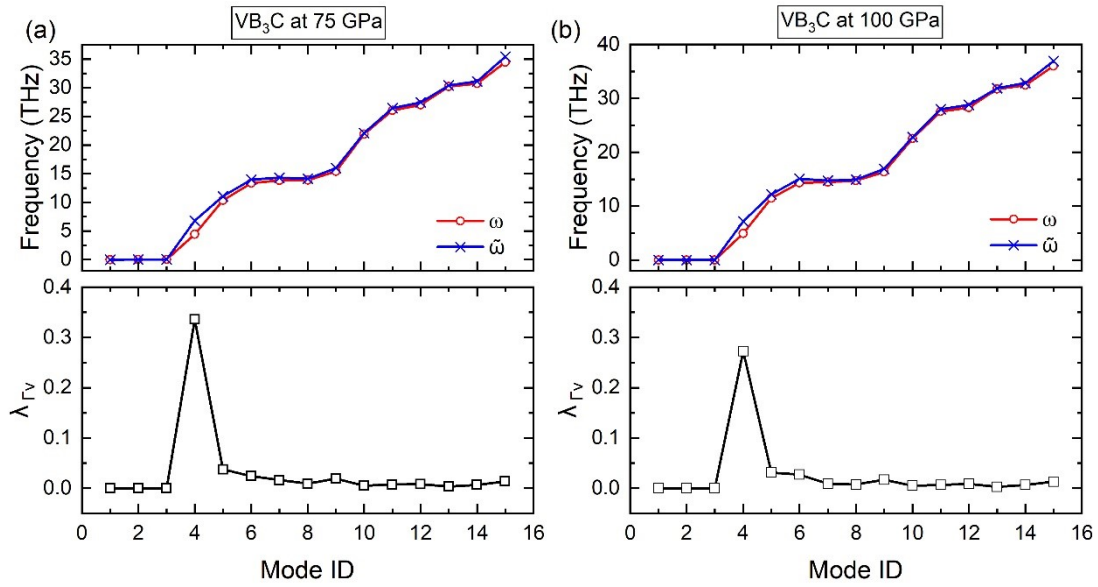

Fig. S4. The screened and unscreened phonon frequency (top panel) and zone-center EPC strength (bottom panel) in VB_3C at (a)75 and (b) 100 GPa.

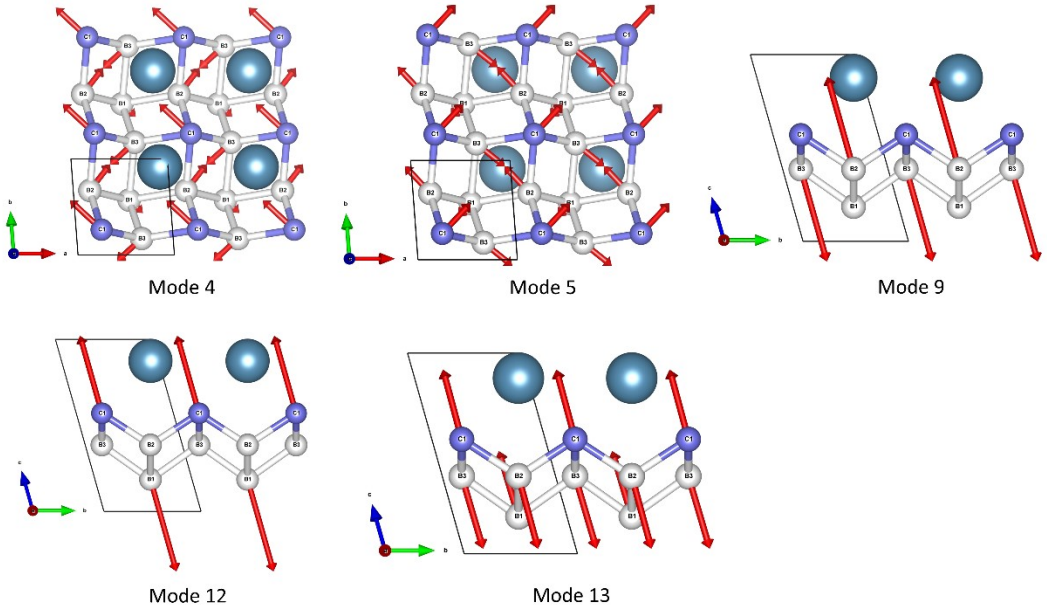

Fig. S5. The vibrational patterns for modes 4, 5, 9, 12, and 13 at the Γ point of CaB_3C at 50 GPa.

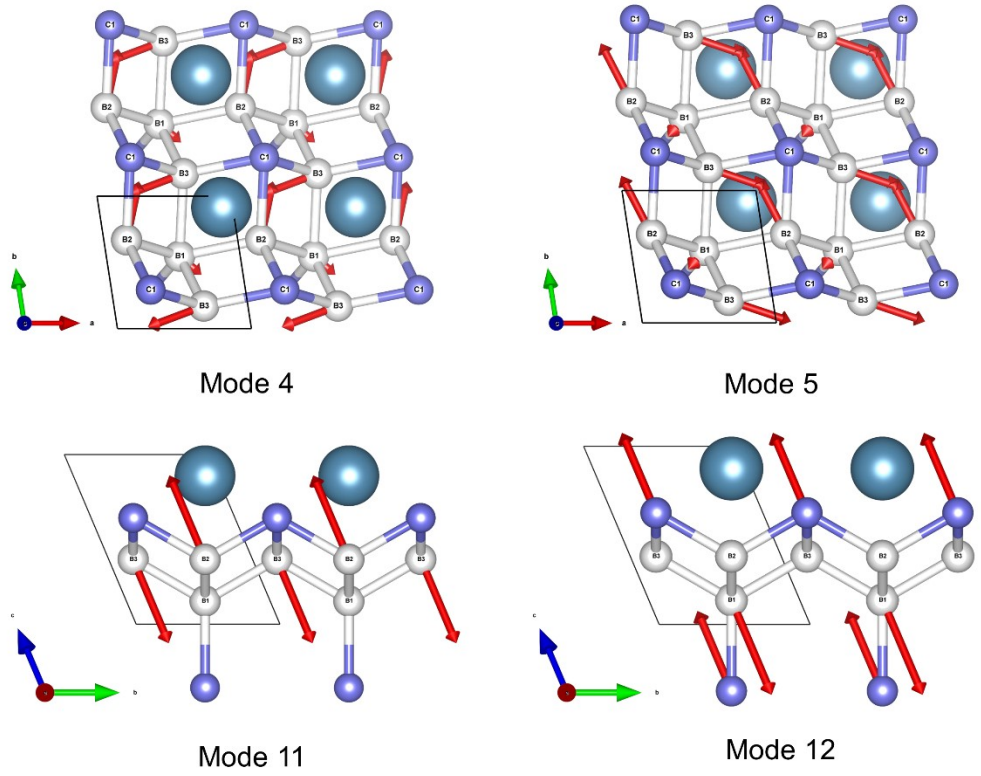

Fig. S6. The vibrational patterns for modes 4, 5,11, and 12 at the Γ point of CaB_3C at 100 GPa.

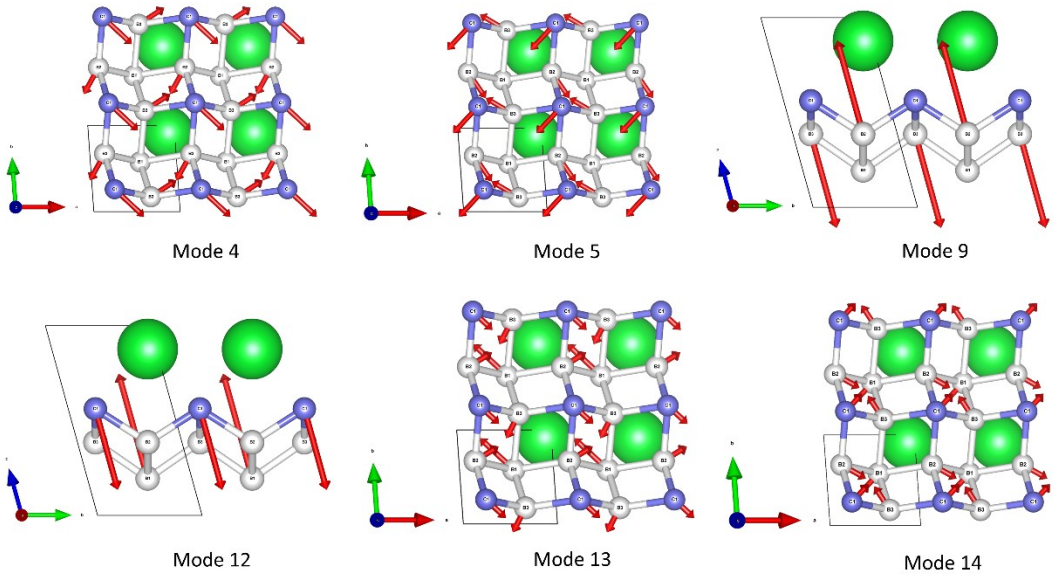

Fig. S7. The vibrational patterns for modes 4, 5, 9, 12, 13, and 14 at the Γ point of SrB_3C at 75 GPa

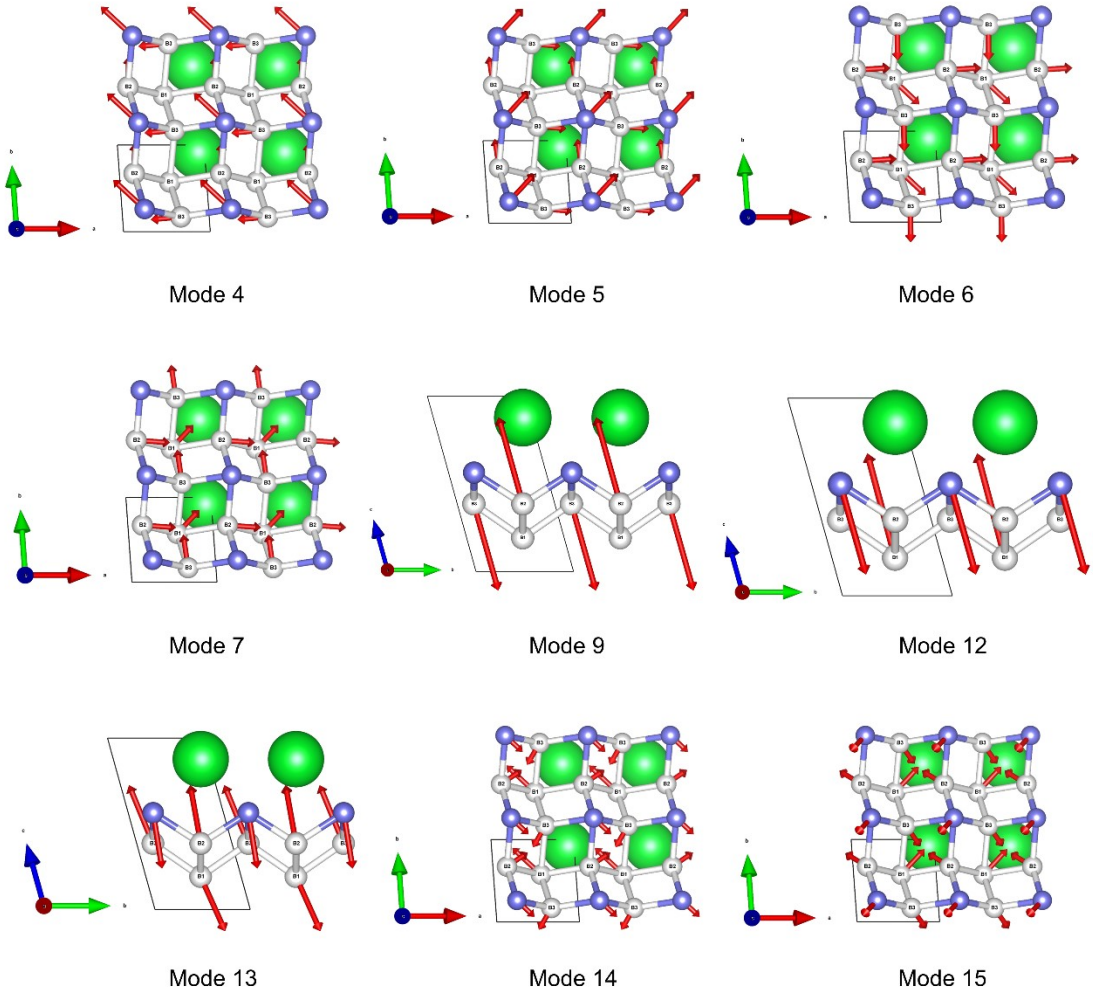

Fig. S8. The vibrational patterns for modes 4, 5, 6, 7, 9, 12, 13, 14, and 15 at the Γ point of SrB_3C at 100 GPa.

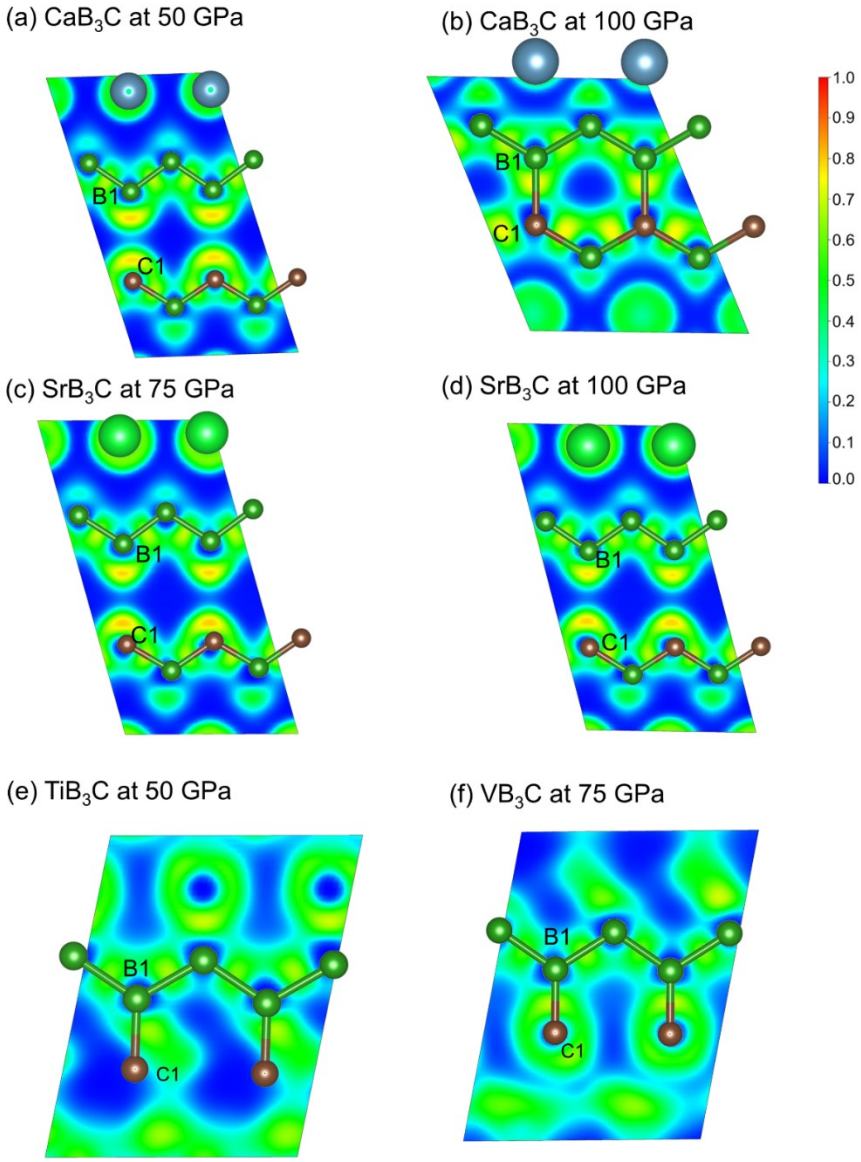

Fig. S9. The electron localization function (ELF) maps of (a) CaB_3C at 50 GPa, (b) CaB_3C at 100 GPa, (c) SrB_3C at 75 GPa, (d) SrB_3C at 100 GPa, (e) TiB_3C at 50 GPa, and (f) VB_3C at 75 GPa.

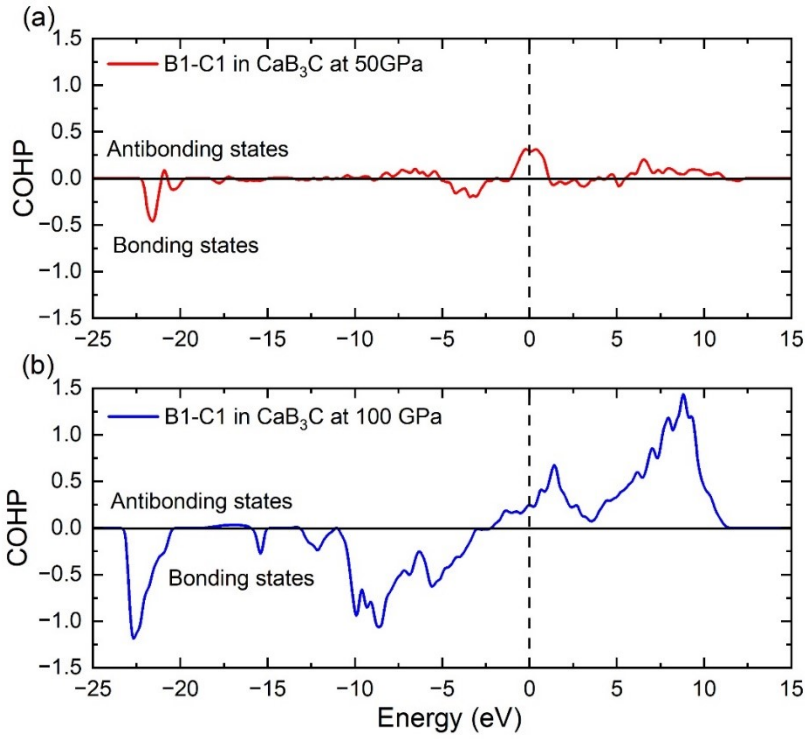

Fig. S10. The COHP for pair B1-C1 in CaB_3C at (a) 50 GPa and (b) 100 GPa.

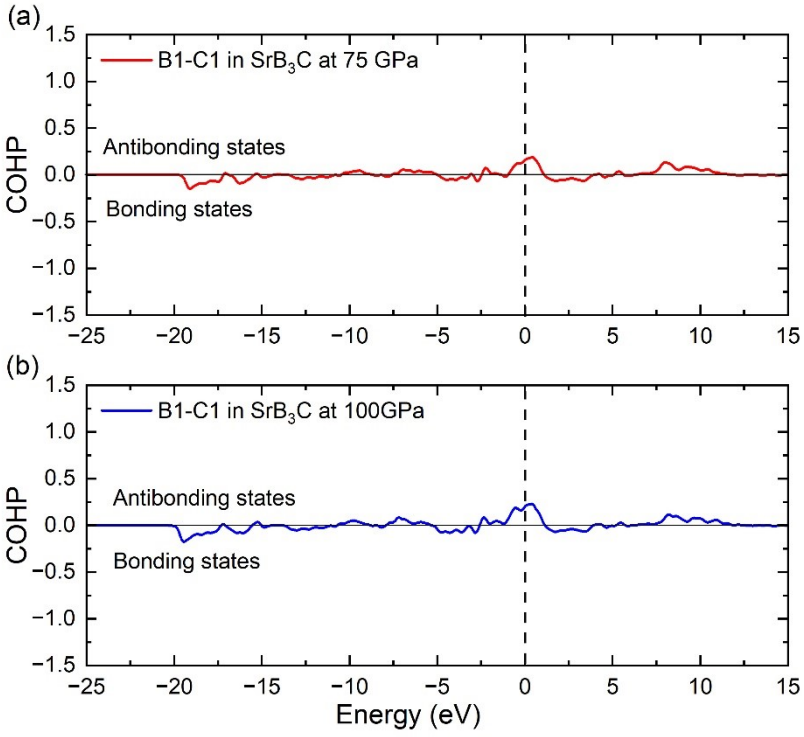

Fig. S11. The COHP for pair B1-C1 in SrB_3C at (a) 75 GPa and (b) 100 GPa.

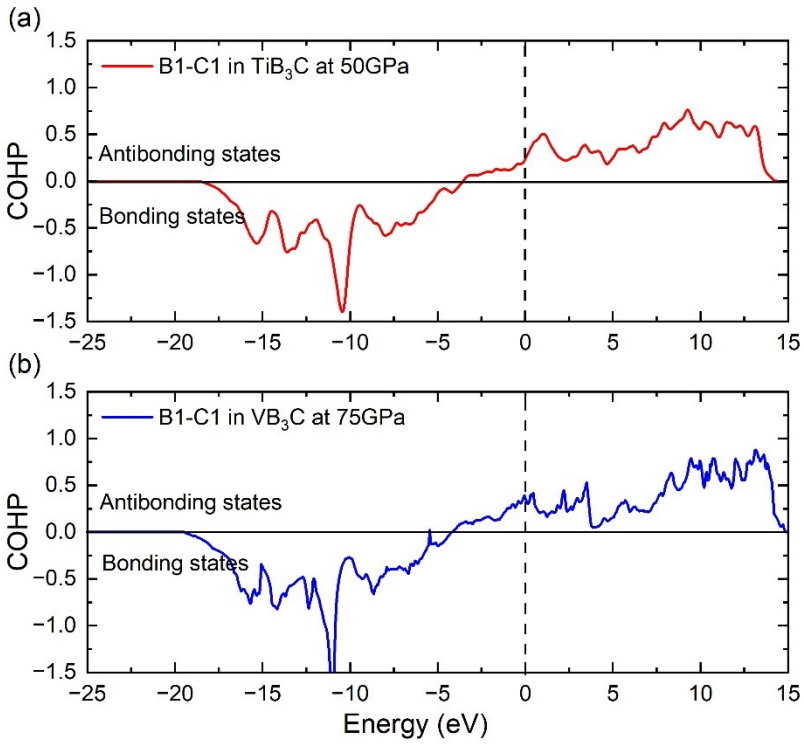

Fig. S12. The COHP for pair B1-C1 in (a) TiB_3C at 50 GPa and VB_3C at 100 GPa.

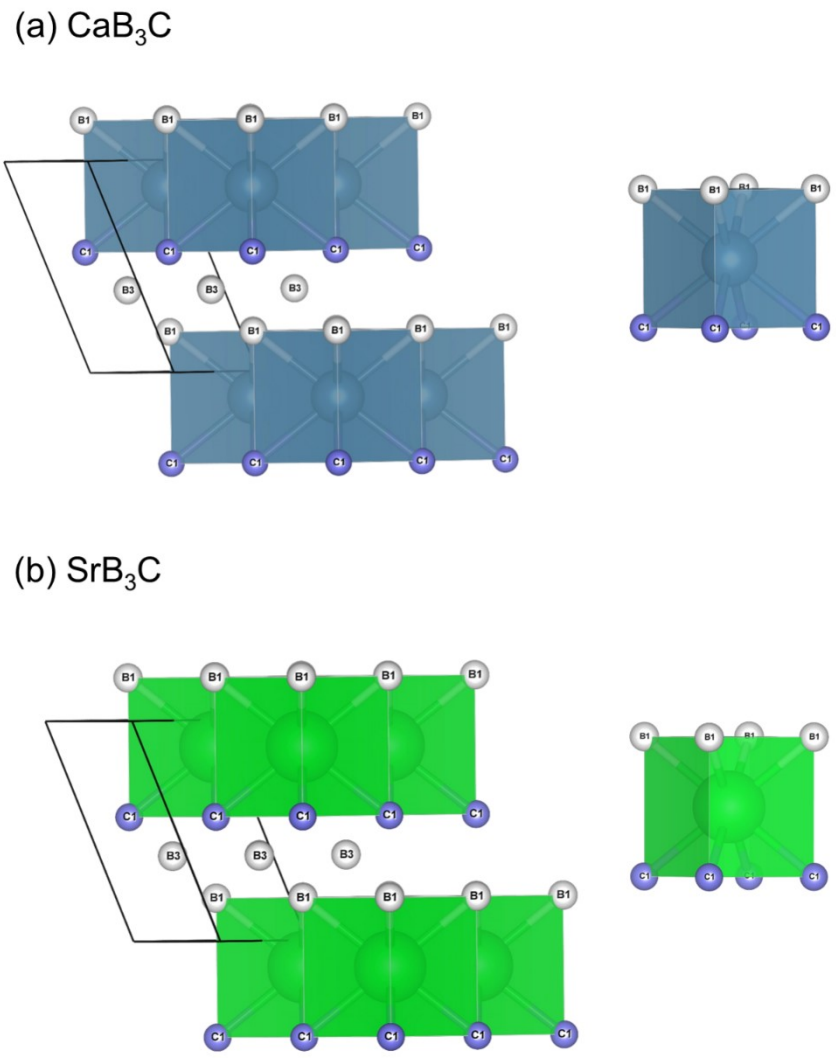

Fig. S13. Crystal structure and coordination polyhedral of (a) CaB_3C and (b) SrB_3C.

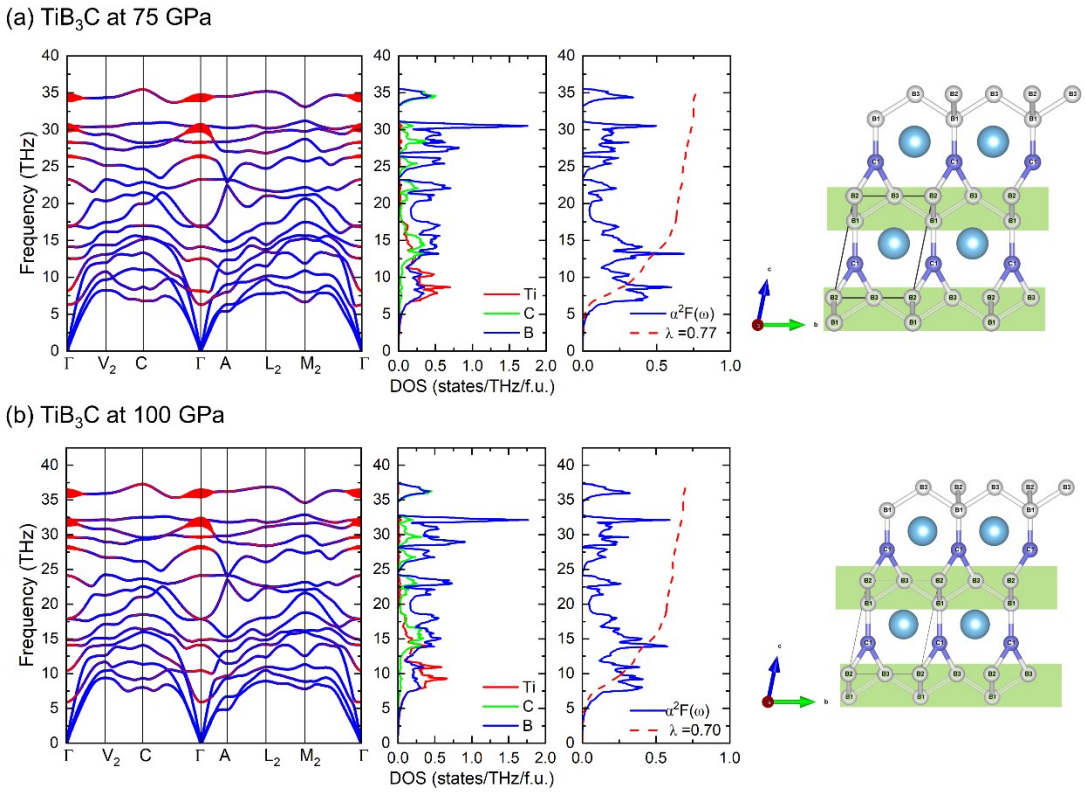

Fig. S14. The γ_{qv}-weighted phonon spectrum, projected phonon density of states (PHDOS), Eliashberg spectral function $\alpha^2F(\omega)$ and crystal structure of TiB_3C at (a) 75 and (b) 100 GPa.

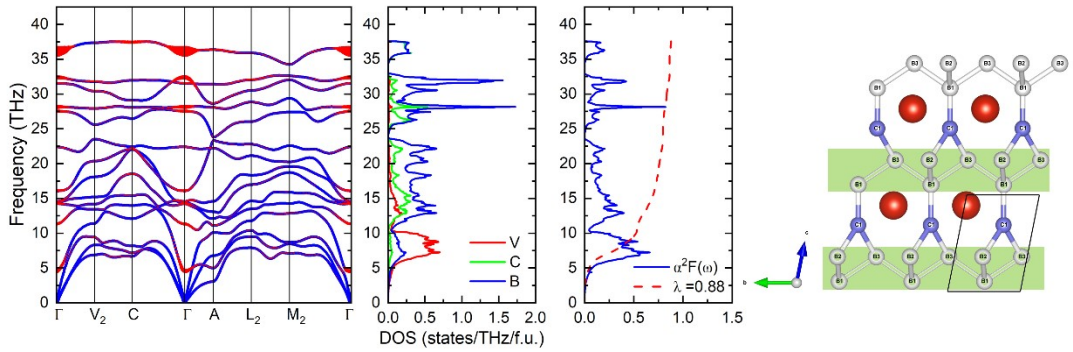

Fig. S15. The γ_{qv}-weighted phonon spectrum, projected phonon density of states (PHDOS), Eliashberg spectral function $\alpha^2F(\omega)$ and crystal structure of VB_3C at 100 GPa.

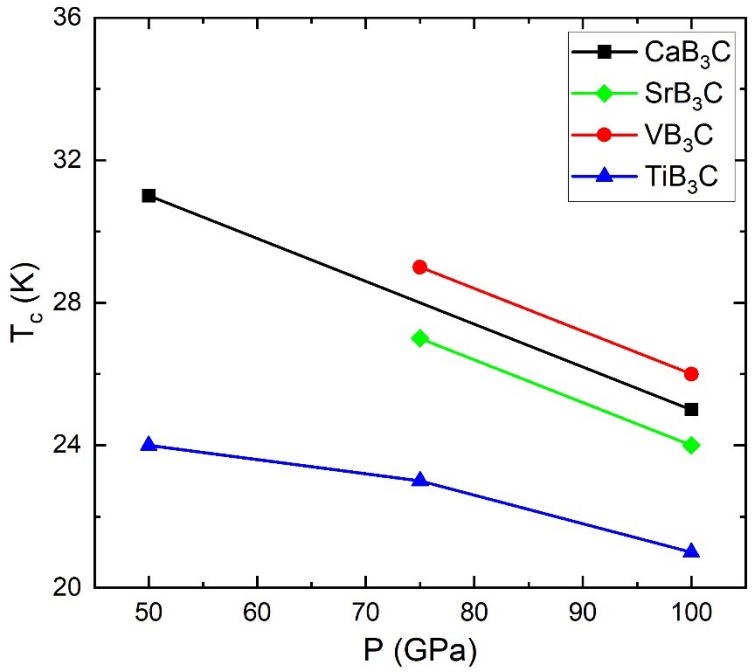

Fig.S16. The pressure-dependence of the T_c of CaB_3C, SrB_3C, TiB_3C, and VB_3C compounds.

Table S1. The covalent radii (Å) of B and C and ionic radii (Å) of Ca, Sr, Ti, and V.

	B	C	Ca	Sr	Ti	V
Covalent radii	0.84	0.76				
Ionic radii (8-coordinate)			1.26	1.40	0.88	0.86